

Corvis Biomechanical Factor Facilitates the Detection of Primary Angle Closure Glaucoma

Chien-Chih Chou¹⁻⁴, Po-Jen Shih⁵, Chun-Yuan Wang², Tzuu-Shuh Jou^{1,6}, Jun-Peng Chen⁷, and I-Jong Wang^{1,8,9}

¹ Graduate Institute of Clinical Medicine, College of Medicine, National Taiwan University, Taipei, Taiwan

² Department of Ophthalmology, Taichung Veterans General Hospital, Taichung, Taiwan

³ School of Medicine, College of Medicine, National Yang Ming Chiao Tung University, Taipei, Taiwan

⁴ Department of Post-Baccalaureate Medicine, College of Medicine, National Chung Hsing University, Taichung, Taiwan

⁵ Department of Biomedical Engineering, National Taiwan University, Taipei, Taiwan

⁶ Center of Precision Medicine, College of Medicine, National Taiwan University, Taipei, Taiwan

⁷ Biostatistics Task Force of Taichung Veterans General Hospital, Taichung, Taiwan

⁸ Graduate Institute of Clinical Medical Science, China Medical University, Taichung, Taiwan

⁹ Department of Ophthalmology, National Taiwan University Hospital, Taipei, Taiwan

Correspondence: I-Jong Wang, Department of Ophthalmology, National Taiwan University Hospital, No.7, Chung-Shan South Road, Taipei, Taiwan.
e-mail: ijong@ms8.hinet.net

Received: April 18, 2022

Accepted: September 9, 2022

Published: October 3, 2022

Keywords: biomechanical properties; Corvis Biomechanical Index; Corvis Biomechanical Factor; primary angle closure glaucoma; anterior chamber volume

Citation: Chou CC, Shih PJ, Wang CY, Jou TS, Chen JP, Wang IJ. Corvis biomechanical factor facilitates the detection of primary angle closure glaucoma. *Transl Vis Sci Technol.* 2022;11(10):7.
<https://doi.org/10.1167/tvst.11.10.7>

Purpose: To characterize the corneal biomechanical properties of primary angle closure glaucoma (PACG) and to investigate the diagnostic performance of combining corneal biomechanical parameters and anterior segment parameters in detecting PACG.

Methods: This retrospective cross-sectional study evaluated 79 and 81 eyes of normal controls and patients with PACG, respectively. Corvis Biomechanical Factor (CBiF) and anterior chamber volume (ACV) were measured using the Corvis ST and Pentacam, respectively. We performed multivariable logistic regression, adjusted for age, sex, central corneal thickness, intraocular pressure, and ACV to evaluate the effect of CBiF on PACG. The area under the receiver operating curve (AUC) was calculated to compare the diagnostic performance of ACV, CBiF, and ACV-CBiF combination for detecting PACG.

Results: The median CBiF of the control and PACG groups was 6.61 (interquartile range [IQR], 6.39–6.88) and 6.20 (IQR, 5.93–6.48), respectively ($P < 0.001$). A lower CBiF, suggestive of decreased corneal biomechanical stability, increased the odds of PACG (odds ratio, 0.029; 95% confidence interval [CI], 0.003–0.266; $P = 0.002$) in the multivariable logistic regression model. The ACV-CBiF combination yielded the highest AUC (0.934; 95% CI, 0.882–0.968) compared with ACV alone (0.878; 95% CI, 0.823–0.928). The ACV-CBiF combination had significantly higher discriminatory ability than that of ACV alone (DeLong test, $P = 0.004$).

Conclusions: Lower CBiF and ACV may act as independent predictors for PACG. Combining ACV and CBiF may enhance detection of PACG.

Translational Relevance: The combination of corneal biomechanical parameters and anterior segment parameters enhances the detection of PACG.

Introduction

Primary angle closure glaucoma (PACG) affects approximately 20 million people aged 40 to 80 years worldwide, and this number is predicted to rise to 32 million by 2040.¹ PACG poses a higher risk of blindness than primary open-angle glaucoma,¹⁻³ although

irreversible visual impairment may be preventable with timely intervention to halt the angle closure process.⁴ PACG often develops insidiously with few symptoms,⁵ thus remaining underdiagnosed,⁶ especially in rural areas.⁷ Hence, it may be beneficial to develop a new classifier for detecting PACG, thereby facilitating prompt patient referral to glaucoma clinics and preventing the irreversible progression of PACG.

The established anterior segment configuration in PACG includes shallow anterior chamber, thick lens, and anteriorly positioned lens.^{2,8,9} Anterior segment imaging modalities such as ultrasound biomicroscopy,¹⁰ anterior segment optical coherence tomography (OCT),^{11,12} swept-source OCT,¹³ and Pentacam¹⁴ provide quantitative imaging-based parameters that can be used to determine the anterior segment configuration.⁴ These parameters have been shown to be effective in detecting PACG.^{12,15,16} However, several factors are involved in the complicated process of angle closure⁴; thus patients having similar values of imaging-based anterior segment parameters may exhibit different clinical manifestations,^{4,17} suggesting limitations when using imaging-based anterior segment parameters alone to detect PACG.^{4,18–21}

In glaucoma studies, corneal biomechanics has attracted increasing attention because it is considered to be a crucial risk factor for the development and progression of primary open-angle glaucoma.^{22,23} Few studies have also investigated corneal biomechanical properties in PACG.^{24,25} The Ocular Response Analyzer (ORA; Reichert Ophthalmic Instruments, Buffalo, NY, USA) is a noncontact tonometer that uses an air puff to indent the central cornea.^{26,27} The ORA uses an infrared beam reflected by the cornea to monitor corneal deformation.²⁷ Corneal hysteresis, a corneal biomechanical property, is measured by the ORA.²⁶ Previous studies have reported lower corneal hysteresis in PACG cases than in normal controls.^{24,25} However, it is unclear whether the combination of corneal biomechanical properties and imaging-based anterior segment parameters would enhance the detection of PACG.

We measured corneal biomechanical properties and anterior segment parameters by using the Corvis ST (Oculus, Wetzlar, Germany) and Pentacam (Oculus), respectively. In this cross-sectional study, we aimed to characterize the corneal biomechanical properties of PACG and ascertain the diagnostic performance of combining corneal biomechanical properties and imaging-based anterior segment parameters in detecting PACG.

Methods

This cross-sectional retrospective study was approved by the Institutional Review Board of National Taiwan University Hospital and followed the tenets of the Declaration of Helsinki. Patients were recruited from National Taiwan University Hospital between October 2017 and February 2021.

The right eye of each patient was used for the study. We reviewed medical images and records retrospectively. PACG was defined as the presence of glaucomatous optic neuropathy coupled with a corresponding visual field defect and angle closure.²⁸ Angle closure was defined as >2 quadrants of invisible posterior trabecular meshwork on nonindentation gonioscopy.²⁶ Glaucomatous optic neuropathy was defined as the presence of a retinal nerve fiber layer defect, vertical cup-to-disc ratio >0.7, cup-to-disc ratio asymmetry >0.2, or neuroretinal rim width <0.1.²⁸ Glaucomatous visual field defect was defined according to the Hodapp-Parrish-Anderson criteria.²⁹ Patients meeting any of the following criteria were excluded: a history of corneal, refractive, cataract, or glaucoma surgery; corneal ulcer; Fuchs' dystrophy; keratoconus; granular dystrophy; corneal edema; Terrien's marginal degeneration; uveitis; secondary angle closure glaucoma; and nonglaucomatous optic neuropathy.

Patients underwent extensive ophthalmic examination, including visual acuity testing, slit-lamp examination, intraocular pressure (IOP) measurement, central corneal thickness (CCT) evaluation, gonioscopy, stereoscopic evaluation of the optic disc, spectral-domain OCT (Cirrus SD-OCT device; Carl Zeiss Meditec, Dublin, CA, USA), visual field examination (Humphrey Visual Field Analyzer II [Carl Zeiss Meditec], using the standard Swedish interactive threshold algorithm with a 24-2 test), anterior segment imaging using Pentacam, and in vivo biomechanical evaluation using Corvis ST. Pentacam uses a rotating Scheimpflug camera to construct three-dimensional images of the anterior segment and to calculate anatomical parameters, including anterior chamber volume (ACV). ACV has high power in detecting narrow angles^{14,30,31} and is significantly correlated with Shaffer angle grading on gonioscopy.¹⁴ In this study, Pentacam software version 1.25r15 was used.

Corvis ST enables in vivo assessment of the dynamic corneal deformation response and corneal biomechanical properties. Corvis ST software version 1.6r2503 was used in this study. The dynamic corneal deformation response incited by a uniaxial air pulse in Corvis ST involves the compression of the extracellular matrix (ECM) and the sliding of corneal collagen lamellae.³² Corvis ST captures high-speed corneal deformation images by using Scheimpflug technology.²² The air pulse emitted from the device forces the normally convex cornea inward into a state of concavity. As the cornea moves inward through the first appplanation, it reaches its highest concavity. This oscillation phase is followed by the returning phase in which the cornea moves outward through a second appplanation before returning to its natural convex shape.

The Corvis ST outputs several intercorrelated parameters that can generate analytical problems such as multiple comparisons and multicollinearity.^{22,33} We selected Corvis Biomechanical Index (CBI) and Corvis Biomechanical Factor (CBiF) as indicators of corneal biomechanical stability. CBI was calculated using a logistic regression algorithm combining different dynamic corneal response parameters obtained from Corvis ST to measure corneal biomechanical stability³⁴ and optimize the discrimination of keratoconus³⁴ and subclinical keratoconus³⁵ from normal corneas. However, CBI is based on a nonlinear model.³⁴ The recent introduction of CBiF has facilitated the linear and standardized assessment of corneal biomechanics.³⁶ CBiF reflects the overall biomechanical stability of the cornea in a linear manner.³⁶ Lower CBiF and higher CBI indicate decreased corneal biomechanical stability.^{34,36} E-stage was defined by classifying CBiF into five stages (E0–E4) to rank the severity of corneal destabilization.³⁷ CBiF values ≥ 5.94 were designated as stage E0. An interval spacing of 0.58 was defined for CBiF gates of each E-stage.³⁷ Lower CBiF values indicated higher E-stages.³⁷ Biomechanically corrected IOP was calculated from finite element simulations that were least affected by corneal properties.³⁸ CCT was measured using Corvis ST Scheimpflug imaging, which has excellent repeatability and accuracy compared with ultrasound pachymetry.³⁹

Statistical Analysis

Statistical analyses were performed using IBM SPSS version 22.0 (IBM Corp., New York, NY, USA). Normality of variables was assessed using the

Kolmogorov-Smirnov test. Nonparametric tests were performed for variables that did not pass the normality test. Continuous variables are presented as median and interquartile range (IQR), and categorical variables are expressed as number and percentage. Differences between the control group and the PACG group were analyzed using the Mann-Whitney *U* test and χ^2 test for continuous and categorical variables, respectively. To identify the predictor variables for PACG, we performed univariable logistic regression analyses. Next, we used multivariable logistic regression analyses adjusted for age, sex, CCT, and IOP to evaluate the effect of the corneal biomechanical parameter (i.e., CBiF) and anatomical anterior segment parameter (i.e., ACV) on PACG. The Wald test was used to determine the significance of the predictor variables. Next, we used MedCalc version 12.0 (MedCalc Software, Ostend, Belgium) for receiver operating characteristic (ROC) analysis. The ROC curve and the area under the ROC curve (AUC) were used to determine the ability of ACV, CBiF, and the ACV–CBiF combination to detect PACG. Optimal cutoffs were chosen to maximize sensitivity and specificity. The DeLong test was used to compare significant differences between the AUCs. All *P* values were two-sided and were considered statistically significant at <0.05 .

Results

In total, 160 eyes of 160 patients were studied—79 from the control group and 81 from the PACG group. The demographic and ophthalmic characteristics of the two groups are summarized in [Table 1](#).

Table 1. Demographic and Ocular Characteristics of Participants

	Control (n = 79)	PACG (n = 81)	<i>P</i> Value
Age (years)	64.0 (56.0, 70.0)	70.0 (67.5, 76.0)	<0.001
Sex*			0.001
Male, no. (%)	39 (49.4%)	18 (22.2%)	
Female, no. (%)	40 (50.6%)	63 (77.8%)	
Average RNFL (μm)	94.00 (89.00, 99.00)	92.00 (80.50, 99.00)	0.061
MD (dB)	-1.16 (-2.13, -0.14)	-3.00 (-6.06, -1.17)	<0.001
PSD (dB)	1.69 (1.39, 2.11)	2.05 (1.59, 3.84)	<0.001
CCT (μm)	559.00 (540.00, 590.00)	541.00 (518.50, 559.00)	<0.001
IOP (mm Hg)	16.50 (14.50, 19.00)	15.50 (13.50, 17.50)	0.006
bIOP (mmHg)	14.60 (12.90, 16.70)	14.00 (12.05, 15.35)	0.061
ACV (mm^3)	123.00 (101.50, 151.25)	77.00 (55.75, 90.25)	<0.001

bIOP, biomechanically corrected intraocular pressure; MD, mean deviation; PSD, pattern standard deviation; RNFL, retinal nerve fiber layer thickness.

Data are presented as median (interquartile range) unless stated otherwise. Mann-Whitney *U* test was used.

* χ^2 test was used.

Table 2. Corneal Biomechanical Parameters Obtained Using Corvis ST

	Control (n = 79)	PACG (n = 81)	P Value
CBI	0.08 (0.03, 0.18)	0.33 (0.14, 0.60)	<0.001
CBiF	6.61 (6.39, 6.88)	6.20 (5.93, 6.48)	<0.001
E-stage	0.00 (0.00, 0.20)	0.50 (0.00, 1.00)	<0.001

Data are presented as median (interquartile range). Mann-Whitney *U* test was used.

The median age of the control and PACG groups was 64.0 (IQR, 56.0–70.0) and 70.0 (IQR, 67.5–76.0) years, respectively ($P < 0.001$). The number of male patients in the control and PACG groups was 39 (49.4%) and 18 (22.2%), respectively ($P = 0.001$). Significant differences in the visual field indexes—including mean deviation and pattern standard deviation—were observed between the two groups ($P < 0.001$). The median CCT of the control and PACG groups was 559.00 (IQR, 540.00–590.00) and 541.00 (IQR, 518.50–559.00) μm , respectively ($P < 0.001$). The median IOP of the control and PACG groups was 16.50 (IQR, 14.50–19.00) and 15.50 (IQR, 13.50–17.50) mm Hg, respectively ($P = 0.006$). No significant difference was observed in biomechanically corrected IOP between the groups. The median ACV of the control and PACG groups was 123.00 (IQR, 101.50–151.25) and 77.00 (IQR, 55.75–90.25) mm^3 , respectively ($P < 0.001$).

The corneal biomechanical parameters obtained using Corvis ST are summarized in Table 2. Significantly higher CBI and lower CBiF values were observed in the PACG group. The median CBI of the control and PACG groups was 0.08 (IQR, 0.03–0.18) and 0.33 (IQR, 0.14–0.60), respectively ($P < 0.001$). The median CBiF of the control and PACG groups was 6.61 (IQR, 6.39–6.88) and 6.20 (IQR, 5.93–6.48), respectively ($P < 0.001$). Furthermore, the median E-stage of the control and PACG groups was 0.00 (IQR, 0.00–0.20) and 0.50 (IQR, 0.00–1.00), respectively ($P < 0.001$).

Table 3 presents the results of univariable and multivariable logistic regression analyses of the effect of ACV and CBiF on PACG. ACV and CBiF were identified as significant predictor variables for PACG in univariable logistic regression analyses. In the multivariable analysis, a lower ACV increased the odds of PACG (odds ratio, 0.950; 95% confidence interval [CI], 0.929–0.971; $P < 0.001$), and a lower CBiF increased the odds of PACG (odds ratio, 0.029; 95% CI, 0.003–0.266; $P = 0.002$).

Table 4 summarizes the results of ROC analyses. The multiparameter classifier comprising CBiF and ACV yielded the highest AUC (0.934; 95% CI, 0.882–0.968) compared with using ACV alone (0.878; 95% CI, 0.823–0.928; Fig.) and CBiF alone (0.799; 95% CI, 0.726–0.860; Fig.). This multiparameter classifier had a significantly higher discriminatory ability than that of ACV alone (DeLong test, $P = 0.004$) and CBiF alone (DeLong test, $P < 0.001$).

Table 3. Logistic Regression Analyses for Predicting Primary Angle Closure Glaucoma

Measurement	Univariable		Multivariable	
	Odds Ratio (95% CI)	P Value	Odds Ratio (95% CI)	P Value
Age (years)	1.120 (1.070–1.173)	<0.001	1.067 (0.982–1.159)	0.126
Sex (Male)	0.293 (0.148–0.581)	<0.001	0.350 (0.100–1.223)	0.100
CCT (μm)	0.980 (0.970–0.990)	<0.001	0.996 (0.974–1.018)	0.700
IOP (mm Hg)	0.898 (0.814–0.991)	0.032	0.959 (0.796–1.154)	0.656
ACV (mm^3)	0.947 (0.931–0.964)	<0.001	0.950 (0.929–0.971)	<0.001
CBiF	0.021 (0.006–0.079)	<0.001	0.029 (0.003–0.266)	0.002

Table 4. Receiver Operating Characteristic Analyses

Variables	AUC	(95% CI)	P Value	Optimal Cutoff	Sensitivity	Specificity
ACV (mm^3)	0.878	(0.823–0.928)	<0.001	>96	86.84%	80.26%
CBiF	0.799	(0.726–0.860)	<0.001	>6.224	51.32%	97.37%
ACV + CBiF	0.934	(0.882–0.968)	<0.001		92.11%	80.26%

The formula used for the multiparameter classifier comprising CBiF and ACV was $\text{Ln}(p/1 - p) = 32.117 - 0.057 \cdot \text{ACV} - 4.119 \cdot \text{CBiF}$.

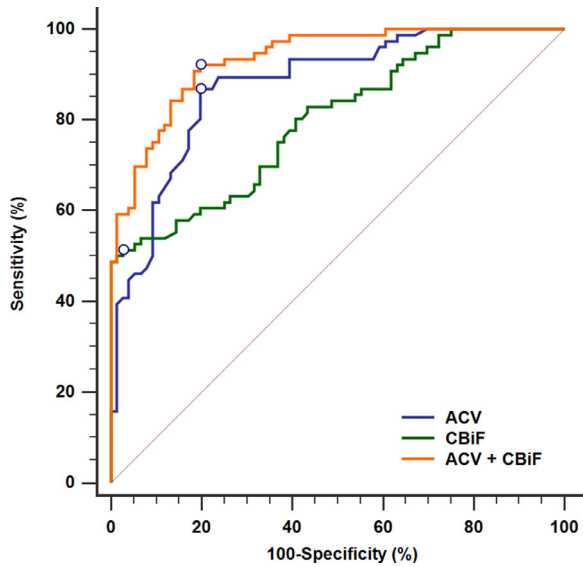


Figure. Receiver operating characteristic curve demonstrated the performance of ACV, CBI-F, and ACV + CBI-F in discriminating between patients with primary angle closure glaucoma and controls. ACV + CBI-F exhibited the highest area under the receiver operating characteristic curve (0.934; 95% CI, 0.882–0.968) compared with ACV alone (0.878; 95% CI, 0.823–0.928) or CBI-F alone (0.799; 95% CI, 0.726–0.860). ACV + CBI-F had significantly higher discriminatory ability than that of ACV alone (DeLong test, $P = 0.004$) and the CBI-F alone (DeLong test, $P < 0.001$).

Discussion

To discern the specific characteristics of PACG, we compared corneal biomechanical properties between patients with PACG and normal controls by using data from Corvis ST. We observed a significantly higher CBI in the PACG group than in the control group. Similarly, Cui et al.⁴⁰ reported higher CBI in eyes with primary angle closure. Because CBI reflects corneal biomechanical stability in a nonlinear manner,³⁴ we further measured CBI-F to evaluate corneal biomechanical stability in a linear manner.³⁶ We observed significantly lower CBI-F, suggestive of decreased corneal biomechanical stability, in the PACG group than in the control group. To explore the role of corneal biomechanical properties in PACG, we performed multivariable logistic regression analyses that included CBI-F, ACV, age, sex, CCT, and IOP as predictor variables for PACG. A lower CBI-F increased the odds of PACG, and a lower ACV increased the odds of PACG. These results highlighted that CBI-F and ACV may act as independent predictors of PACG.

We performed ROC analyses to investigate whether combining CBI-F and ACV improved the detection of PACG. For ACV alone, we obtained an AUC value of 0.878 (95% CI, 0.823–0.928). A previous

study similarly reported that ACV alone yielded an AUC value of 0.89 in identifying angle closure.³¹ The formula used for the multiparameter classifier comprising CBI-F and ACV was $\text{Ln}(p/1 - p) = 32.117 - 0.057 \cdot \text{ACV} - 4.119 \cdot \text{CBI-F}$. We observed that the multiparameter classifier yielded the highest AUC (0.934; 95% CI, 0.882–0.968). This multiparameter classifier also had a significantly higher discriminatory ability than ACV alone ($P = 0.004$ using DeLong test). This finding suggests that incorporating biomechanical properties such as CBI-F in clinical settings is beneficial for detecting PACG.

Corneal biomechanics reflects the biomechanical properties of the ECM.^{41–43} Studies have demonstrated that single nucleotide polymorphisms in matrix metalloproteinase 9, which drives ECM remodeling, could be associated with PACG pathogenesis.⁴⁴ Furthermore, two genome-wide association studies have identified ECM-related susceptibility loci for PACG, including EPDR1 and COL11A1.^{45,46} EPDR1 encodes ependymin-related protein 1, which is an antiadhesive molecule and is active within the collagen fibrils of the ECM.⁴⁷ COL11A1 encodes alpha chains of type XI collagen, an essential component of the ECM.⁴⁷ In addition, the expression of collagen I and secreted protein acidic and rich in cysteine is high in patients with PACG.¹⁷ Secreted protein acidic and rich in cysteine mediates collagen deposition and changes the biomechanical properties of the ECM.¹⁷ Taken together, these findings indicate that an abnormal ECM in eyes with PACG may cause decreased corneal biomechanical stability.

Corneal biomechanical properties may reflect whole-eye biomechanical properties.^{22,23,48} Similarities between the ECM constituents of the cornea, anterior segment, peripapillary sclera, and lamina cribrosa may imply similar biomechanical properties of these ocular structures.^{41,42} Studies have demonstrated that the dynamic corneal response parameters obtained using Corvis ST are closely correlated with scleral biomechanical properties^{23,48} and the posterior pole profile.²³ Accordingly, decreased corneal biomechanical stability in PACG may also indicate decreased biomechanical stability of the anterior segment, peripapillary sclera, and lamina cribrosa.

In PACG, anterior segment structures with decreased biomechanical stability may deform easily, altering the dynamic interaction between the iris and peripheral cornea. With a crowded anterior segment and occludable iridocorneal angle, the decreased biomechanical stability of the anterior segment may precipitate more extensive and frequent iridotrabecular contact, which would impede access of the aqueous to the trabecular meshwork, causing increased IOP

and progression to glaucomatous optic neuropathy. This mechanism may explain the role of lower CBI_F in PACG.

The lamina cribrosa and peripapillary sclera in the posterior pole are the main load-bearing structures of the optic disc.⁴⁹ Decreased biomechanical stability of the peripapillary sclera and lamina cribrosa may lead to the mechanical environment characteristic of the optic disc,^{50,51} as well as the extent of peripapillary atrophy in PACG.⁵² Consistently, Nouri-Mahdavi et al.⁵³ revealed characteristic patterns of glaucomatous disc damage and visual field defects in PACG.

Corneal hysteresis obtained from the ORA reflects the capacity of the cornea to dissipate energy.²⁶ Previous studies have reported lower corneal hysteresis in patients with PACG than in normal controls.^{24,25} Hussnain et al.⁵⁴ also reported that corneal hysteresis was not correlated with anatomical anterior segment parameters obtained from anterior segment OCT. Our findings extend those of previous studies and provide a comprehensive understanding of the role of corneal biomechanical properties in PACG.

This study has several limitations. First, patients were enrolled from a tertiary-care academic hospital. This may limit the generalization of our results to PACG in the broader population. Second, our study population was exclusively Asian. Future studies involving other ethnicities are therefore required. Third, antiglaucoma medication history was not evaluated in our study because of the inconsistent effects of antiglaucoma medication on corneal biomechanics.^{55–57} In addition, different prostaglandin analogues may exert different levels of effects on corneal biomechanics.⁵⁸ Last, deriving causal relationships was difficult because of our cross-sectional study design. Future longitudinal cohort studies are warranted to elucidate causality and determine the correlation between biomechanical parameters and disease progression.

In summary, we demonstrated the lower CBI_F and lower ACV may serve as independent predictors of PACG. The combination of CBI_F and ACV may also enhance the detection of PACG. Our findings provide a unique conceptual framework for understanding PACG.

Acknowledgments

Supported by Ministry of Science and Technology of Taiwan (MOST 110-2634-F-002-044) and Taichung Veterans General Hospital (TCVGH-1106903B). The

authors have no financial conflict of interest. This manuscript was edited by Wallace Academic Editing.

Disclosure: **C.-C. Chou**, None; **P.-J. Shih**, None; **C.-Y. Wang**, None; **T.-S. Jou**, None; **J.-P. Chen**, None; **I.-J. Wang**, None

References

1. Tham YC, Li X, Wong TY, Quigley HA, Aung T, Cheng CY. Global prevalence of glaucoma and projections of glaucoma burden through 2040: a systematic review and meta-analysis. *Ophthalmology*. 2014;121:2081–2090.
2. Friedman DS, Foster PJ, Aung T, He M. Angle closure and angle-closure glaucoma: what we are doing now and what we will be doing in the future. *Clin Exp Ophthalmol*. 2012;40:381–387.
3. Quigley HA, Broman AT. The number of people with glaucoma worldwide in 2010 and 2020. *Br J Ophthalmol*. 2006;90:262.
4. Sun X, Dai Y, Chen Y, et al. Primary angle closure glaucoma: What we know and what we don't know. *Prog Retin Eye Res*. 2017;57:26–45.
5. Jindal A, Ctori I, Virgili G, Lucenteforte E, Lawrenson JG. Non-contact tests for identifying people at risk of primary angle closure glaucoma. *Cochrane Database Syst Rev*. 2020;5(5):Cd012947.
6. Michelessi M, Azuara-Blanco A, Virgili G. Cochrane Corner: evidence on the management of primary angle closure glaucoma. *Eye*. 2022;36:684–685.
7. Liang Y, Friedman DS, Zhou Q, et al. Prevalence and characteristics of primary angle-closure diseases in a rural adult Chinese population: the Handan Eye Study. *Invest Ophthalmol Vis Sci*. 2011;52:8672–8679.
8. Aung T, Nolan WP, Machin D, et al. Anterior chamber depth and the risk of primary angle closure in 2 East Asian populations. *Arch Ophthalmol*. 2005;123:527–532.
9. Wojciechowski R, Congdon N, Anninger W, Teo Broman A. Age, gender, biometry, refractive error, and the anterior chamber angle among Alaskan Eskimos. *Ophthalmology*. 2003;110:365–375.
10. Pavlin CJ, Ritch R, Foster FS. Ultrasound biomicroscopy in plateau iris syndrome. *Am J Ophthalmol*. 1992;113:390–395.
11. Nolan WP, See JL, Chew PT, et al. Detection of primary angle closure using anterior segment optical coherence tomography in Asian eyes. *Ophthalmology*. 2007;114(1):33–39.

12. Nongpiur ME, He M, Amerasinghe N, et al. Lens vault, thickness, and position in Chinese subjects with angle closure. *Ophthalmology*. 2011;118:474–479.
13. Mak H, Xu G, Leung CK. Imaging the iris with swept-source optical coherence tomography: relationship between iris volume and primary angle closure. *Ophthalmology*. 2013;120:2517–2524.
14. Kurita N, Mayama C, Tomidokoro A, Aihara M, Araie M. Potential of the pentacam in screening for primary angle closure and primary angle closure suspect. *J Glaucoma*. 2009;18:506–512.
15. Wu RY, Nongpiur ME, He MG, et al. Association of narrow angles with anterior chamber area and volume measured with anterior-segment optical coherence tomography. *Arch Ophthalmol*. 2011;129:569–574.
16. Nongpiur ME, Khor CC, Cheng CY, et al. Integration of genetic and biometric risk factors for detection of primary angle closure glaucoma. *Am J Ophthalmol*. 2019;208:160–165.
17. Chua J, Seet LF, Jiang Y, et al. Increased SPARC expression in primary angle closure glaucoma iris. *Mol Vision*. 2008;14:1886–1892.
18. Thomas R, George R, Parikh R, Muliylil J, Jacob A. Five year risk of progression of primary angle closure suspects to primary angle closure: a population based study. *Br J Ophthalmol*. 2003;87:450–454.
19. Thomas R, Parikh R, Muliylil J, Kumar RS. Five-year risk of progression of primary angle closure to primary angle closure glaucoma: a population-based study. *Acta Ophthalmol Scand*. 2003;81:480–485.
20. Peng PH, Nguyen H, Lin HS, Nguyen N, Lin S. Long-term outcomes of laser iridotomy in Vietnamese patients with primary angle closure. *Br J Ophthalmol*. 2011;95:1207–1211.
21. Nongpiur ME, Cheng CY, Duvessh R, et al. Evaluation of primary angle-closure glaucoma susceptibility loci in patients with early stages of angle-closure disease. *Ophthalmology*. 2018;125:664–670.
22. Qassim A, Mullany S, Abedi F, et al. Corneal stiffness parameters are predictive of structural and functional progression in glaucoma suspect eyes. *Ophthalmology*. 2020;128:993–1004.
23. Jung Y, Park HY, Park CK. Association between corneal deformation amplitude and posterior pole profiles in primary open-angle glaucoma. *Ophthalmology*. 2016;123:959–964.
24. Narayanaswamy A, Su DH, Baskaran M, et al. Comparison of ocular response analyzer parameters in chinese subjects with primary angle-closure and primary open-angle glaucoma. *Arch Ophthalmol*. 2011;129:429–434.
25. Sun L, Shen M, Wang J, et al. Recovery of corneal hysteresis after reduction of intraocular pressure in chronic primary angle-closure glaucoma. *Am J Ophthalmol*. 2009;147:1061–1066.
26. Nongpiur ME, Png O, Chiew JW, et al. Lack of association between corneal hysteresis and corneal resistance factor with glaucoma severity in primary angle closure glaucoma. *Invest Ophthalmol Vis Sci*. 2015;56:6879–6885.
27. Esporcatte LPG, Salomão MQ, Lopes BT, et al. Biomechanical diagnostics of the cornea. *Eye Vis (Lond)*. 2020;7:9.
28. Foster PJ, Buhrmann R, Quigley HA, Johnson GJ. The definition and classification of glaucoma in prevalence surveys. *Br J Ophthalmol*. 2002;86:238–242.
29. Hodapp E, Parrish RK, Anderson DR. *Clinical decisions in glaucoma*. St. Louis: Mosby; 1993.
30. Grewal DS, Brar GS, Jain R, Grewal SPS. Comparison of Scheimpflug imaging and spectral domain anterior segment optical coherence tomography for detection of narrow anterior chamber angles. *Eye (Lond)*. 2011;25:603–611.
31. Rossi GC, Scudeller L, Delfino A, et al. Pentacam sensitivity and specificity in detecting occludable angles. *Eur J Ophthalmol*. 2012;22:701–708.
32. Ye C, Yu M, Lai G, Jhanji V. Variability of corneal deformation response in normal and keratoconic eyes. *Optom Vis Sci*. 2015;92:e149–e153.
33. Vinciguerra R, Elsheikh A, Roberts CJ, et al. Influence of pachymetry and intraocular pressure on dynamic corneal response parameters in healthy patients. *J Refract Surg*. 2016;32:550–561.
34. Vinciguerra R, Ambrosio R, Jr., Elsheikh A, et al. Detection of keratoconus with a new biomechanical index. *J Refract Surg*. 2016;32:803–810.
35. Vinciguerra R, Ambrósio R, Jr., Roberts CJ, Azzolini C, Vinciguerra P. Biomechanical characterization of subclinical keratoconus without topographic or tomographic abnormalities. *J Refract Surg*. 2017;33:399–407.
36. Flockerzi E, Vinciguerra R, Belin MW, Vinciguerra P, Ambrósio R, Jr., Seitz B. Correlation of the Corvis Biomechanical Factor with tomographic parameters in keratoconus. *J Cataract Refract Surg*. 2022;48:215–221.
37. Flockerzi E, Vinciguerra R, Belin MW, Vinciguerra P, Ambrósio R, Jr., Seitz B. Combined biomechanical and tomographic keratoconus staging: Adding a biomechanical parameter to the ABCD keratoconus staging system. *Acta Ophthalmol*. 2022;100(5):e1135–e1142.

38. Joda AA, Shervin MM, Kook D, Elsheikh A. Development and validation of a correction equation for Corvis tonometry. *Comput Methods Biomech Biomed Eng.* 2016;19:943–953.
39. Reznicek L, Muth D, Kampik A, Neubauer AS, Hirneiss C. Evaluation of a novel Scheimpflug-based non-contact tonometer in healthy subjects and patients with ocular hypertension and glaucoma. *Br J Ophthalmol.* 2013;97:1410.
40. Cui X, Yang Y, Li Y, et al. Correlation between anterior chamber volume and corneal biomechanical properties in human eyes. *Front Bioeng Biotechnol.* 2019;7:379.
41. Kotecha A. What biomechanical properties of the cornea are relevant for the clinician? *Surv Ophthalmol.* 2007;52(Suppl 2):S109–S114.
42. Marshall GE, Konstas AG, Lee WR. Collagens in ocular tissues. *Br J Ophthalmol.* 1993;77:515–524.
43. Cox TR, Erler JT. Remodeling and homeostasis of the extracellular matrix: implications for fibrotic diseases and cancer. *Dis Model Mech.* 2011;4:165–178.
44. Wang IJ, Chiang TH, Shih YF, et al. The association of single nucleotide polymorphisms in the MMP-9 genes with susceptibility to acute primary angle closure glaucoma in Taiwanese patients. *Mol Vision.* 2006;12:1223–1232.
45. Vithana EN, Khor CC, Qiao C, et al. Genome-wide association analyses identify three new susceptibility loci for primary angle closure glaucoma. *Nat Genet.* 2012;44:1142–1146.
46. Khor CC, Do T, Jia H, et al. Genome-wide association study identifies five new susceptibility loci for primary angle closure glaucoma. *Nat Genet.* 2016;48:556–562.
47. Liu C, Nongpiur ME, Cheng CY, et al. Evaluation of primary angle-closure glaucoma susceptibility loci for estimating angle closure disease severity. *Ophthalmology.* 2021;128:403–409.
48. Nguyen BA, Reilly MA, Roberts CJ. Biomechanical contribution of the sclera to dynamic corneal response in air-puff induced deformation in human donor eyes. *Exp Eye Res.* 2020;191:107904.
49. Sigal IA, Yang H, Roberts MD, Burgoyne CF, Downs JC. IOP-induced lamina cribrosa displacement and scleral canal expansion: an analysis of factor interactions using parameterized eye-specific models. *Invest Ophthalmol Vis Sci.* 2011;52:1896–1907.
50. Sigal IA, Flanagan JG, Ethier CR. Factors influencing optic nerve head biomechanics. *Invest Ophthalmol Vis Sci.* 2005;46:4189–4199.
51. Boote C, Sigal IA, Grytz R, Hua Y, Nguyen TD, Girard MJA. Scleral structure and biomechanics. *Prog Retin Eye Res.* 2020;74:100773.
52. Uchida H, Yamamoto T, Tomita G, Kitazawa Y. Peripapillary atrophy in primary angle-closure glaucoma: a comparative study with primary open-angle glaucoma. *Am J Ophthalmol.* 1999;127:121–128.
53. Nouri-Mahdavi K, Supawavej C, Bitrian E, et al. Patterns of damage in chronic angle-closure glaucoma compared to primary open-angle glaucoma. *Am J Ophthalmol.* 2011;152:74–80.
54. Hussnain SA, Kovacs KD, Warren JL, Teng CC. Corneal hysteresis and anterior segment optical coherence tomography anatomical parameters in primary angle closure suspects. *Clin Exp Ophthalmol.* 2018;46:468–472.
55. Meda R, Wang Q, Paoloni D, Harasymowycz P, Brunette I. The impact of chronic use of prostaglandin analogues on the biomechanical properties of the cornea in patients with primary open-angle glaucoma. *Br J Ophthalmol.* 2017;101:120.
56. Bolívar G, Sánchez-Barahona C, Teus M, et al. Effect of topical prostaglandin analogues on corneal hysteresis. *Acta Ophthalmol.* 2015;93(6):e495–e498.
57. Wu N, Chen Y, Yang Y, Sun X. The changes of corneal biomechanical properties with long-term treatment of prostaglandin analogue measured by Corvis ST. *BMC Ophthalmol.* 2020;20(1):422–422.
58. Wang J, Zhao Y, Yu A, et al. Effect of travoprost, latanoprost and bimatoprost PGF₂ α treatments on the biomechanical properties of in-vivo rabbit cornea. *Exp Eye Res.* 2022;215:108920.